BBA - Bioenergetics 1860 (2019) 189–200

Contents lists available at ScienceDirect

BBA - Bioenergetics

journal homepage: www.elsevier.com/locate/bbabio

Structure-dynamic and functional relationships in a Li^+-transporting sodium-calcium exchanger mutant

Moshe Giladi[a,1], Su Youn Lee[b,1], Bosmat Refaeli[a,1], Reuben Hiller[a], Ka Young Chung[b,*], Daniel Khananshvili[a,*]

[a] Department of Physiology and Pharmacology, Sackler School of Medicine, Tel-Aviv University, Tel-Aviv 69978, Israel
[b] School of Pharmacy, Sungkyunkwan University, Jangan-gu, Suwon 16419, South Korea

ARTICLE INFO

Keywords:
Mitochondrial NCLX
Transporter
HDX-MS
Ion selectivity
Lithium
Alternating access

ABSTRACT

The cell membrane (NCX) and mitochondrial (NCLX) Na^+/Ca^{2+} exchangers control Ca^{2+} homeostasis. Eleven (out of twelve) ion-coordinating residues are highly conserved among eukaryotic and prokaryotic NCXs, whereas in NCLX, nine (out of twelve) ion-coordinating residues are different. Consequently, NCXs exhibit high selectivity for Na^+ and Ca^{2+}, whereas NCLX can exchange Ca^{2+} with either Na^+ or Li^+. However, the underlying molecular mechanisms and physiological relevance remain unresolved. Here, we analyzed the NCX_Mj-derived mutant NCLX_Mj (with nine substituted residues) imitating the ion selectivity of NCLX. Site-directed fluorescent labeling and ion flux assays revealed the nearly symmetric accessibility of ions to the extracellular and cytosolic vestibules in NCLX_Mj (K_{int} = 0.8–1.4), whereas the extracellular vestibule is predominantly accessible to ions (K_{int} = 0.1–0.2) in NCX_Mj. HDX-MS (hydrogen-deuterium exchange mass-spectrometry) identified symmetrically rigidified core helix segments in NCLX_Mj, whereas the matching structural elements are asymmetrically rigidified in NCX_Mj. The HDX-MS analyses of ion-induced conformational changes and the mutational effects on ion fluxes revealed that the "Ca^{2+}-site" (S_{Ca}) of NCLX_Mj binds Na^+, Li^+, or Ca^{2+}, whereas one or more additional Na^+/Li^+ sites of NCLX_Mj are incompatible with the Na^+ sites (S_{ext} and S_{int}) of NCX_Mj. Thus, the replacement of ion-coordinating residues in NCLX_Mj alters not only the ion selectivity of NCLX_Mj, but also the capacity and affinity for Na^+/Li^+ (but not for Ca^{2+}) binding, bidirectional ion-accessibility, the response of the ion-exchange to membrane potential changes, and more. These structure-controlled functional features could be relevant for differential contributions of NCX and NCLX to Ca^{2+} homeostasis in distinct sub-cellular compartments.

1. Introduction

The cell membrane (NCX) and mitochondrial (NCLX) Na^+/Ca^{2+} exchangers represent distinct molecular entities that are exposed to diverse ionic concentrations, electrochemical gradients, and membrane potentials in distinct subcellular compartments [1–4]. The NCX and NCLX proteins belong to the Ca/CA (Ca^{2+}/Cation Antiporter) superfamily, where the NCX, NCLX, NCKX, and CAX gene families mediate the bidirectional movements of different monovalent ions (Na^+, K^+, Li^+, or H^+) in exchange with the Ca^{2+} ion [3–8]. Despite their differences in ion selectivity, the Ca/CA proteins share some common structural motifs, which may represent a universal mechanism underlying ion-coupled alternating access [7–9]. Notably, the Ca/CA proteins exhibit inverted twofold asymmetry (Fig. 1A,B), where highly conserved ion-coordinating residues (on the α_1 and α_2 repeats) control the ion transport rates, which is secondarily modulated by regulatory domains [8–12]. Resolution of the structure-dynamic determinants governing ion selectivity is especially challenging with respect to ion-coupled transport mechanisms [13–16].

Eukaryotic and prokaryotic NCXs extrude $1Ca^{2+}$ in exchange with $3Na^+$ [17–19], where the Na^+- and Ca^{2+}-bound species are separately transported along the transport cycle [20]. The crystal structure of NCX_Mj (from Methanococcus jannaschii) revealed ten transmembrane helices (TM1–10), where twelve ion-coordinating residues (located in the α-repeats on TM2, TM3, TM7, and TM8) form four binding sites: S_{ext}, S_{mid}, S_{int}, and S_{Ca} [21] (Fig. 1). Eleven ion-coordinating residues (out of twelve) are identical in eukaryotic NCXs and NCX_Mj, thus suggesting that in the absence of the crystal structure of eukaryotic NCX

* Corresponding authors.
E-mail addresses: kychung2@skku.edu (K.Y. Chung), dhanan@post.tau.ac.il (D. Khananshvili).
[1] These authors contributed equally.

https://doi.org/10.1016/j.bbabio.2018.11.015
Received 16 May 2018; Received in revised form 27 August 2018; Accepted 7 November 2018
Available online 08 November 2018

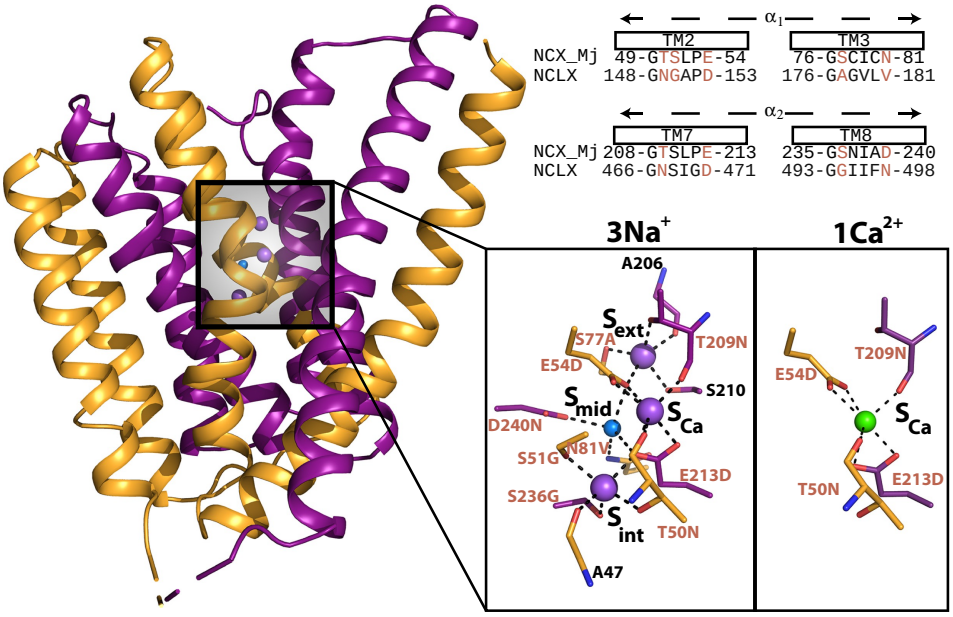

Fig. 1. Structure of NCX_Mj. The structure of $3Na^+$-bound NCX_Mj (PDB 5HXE) is presented as a cartoon, with the symmetry-related halves in orange (helices 1–5) and purple (helices 6–10). Sequence alignments of the α-repeats from NCX_Mj and NCLX are shown, and mutated residues are in red. A close-up of the ion binding sites is shown, depicting ion-coordinating residues as sticks. Purple, blue, and green spheres represent Na^+, water, and Ca^{2+}, respectively.

and NCLX, the structural template of NCX_Mj may serve as a useful model for studying the ion transport mechanisms in NCX and NCLX [22–25]. Notably, the structural data [26–29] support the notion that the Ca/CA proteins share a common mechanism for ion-coupled alternating access, despite the fact that they mediate the transport of distinct monovalent ions in exchange with calcium [2–9].

Molecular dynamics (MD) simulations and ion flux analyses of single-point mutations of ion-coordinating residues in NCX_Mj [23,25] revealed that $3Na^+$ ions occupy S_{ext}, S_{int}, and S_{Ca}, whereas $1Ca^{2+}$ occupies S_{Ca} (Fig. 1). This conclusion was confirmed in a recent crystallographic study [26]. Thus, the S_{int} and S_{ext} sites are highly selective to Na^+, whereas S_{Ca} can bind either Na^+ or Ca^{2+}. Although there is no evidence for Na^+ or Ca^{2+} binding to S_{mid} in NCXs, this site may bind water in the ground state [25,26], although D240 (at S_{mid}) is involved in ion-transport catalysis, probably because it stabilizes the ion-bound species in the transition state [23]. In terms of ion selectivity, the mitochondrial NCLX exhibits quite exceptional features among NCXs, since it can exchange Ca^{2+} with either Na^+ or Li^+ [30]. Notably, nine (out of twelve) ion-coordinating residues differ between NCLX and NCX_Mj [4,8,16]. However, it remains unclear how the structural differences in the ion-coordinating residues can contribute to ion binding selectivity, capacity, and affinity and how all of them are related to the huge differences in the transport cycle turnover rates [3,7–9,16]. To imitate the Li^+ transport activity, we have recently performed structure-based replacement of nine ion-coordinating residues in NCX_Mj (Fig. 1) and found that the designed NCLX_Mj can transport Ca^{2+} in exchange with either Na^+ or Li^+ [31].

The present study was undertaken to analyze the structure-dynamic features of apo and ion-bound NCLX_Mj, with the goal of detecting conformational differences between NCX_Mj and NCLX_Mj at specific sites with or without Na^+, Li^+, or Ca^{2+}. The site-directed labeling of cysteine residues (placed at specific locations within the extracellular and cytosolic vestibules) was done by using TMRM (tetramethylrhodamine-5-maleimide) [24,32,33]. Hydrogen-deuterium exchange mass spectrometry (HDX-MS) [22–24,34–36] was explored, with the goal of identifying the characteristic features of local backbone dynamics in the apo and ion-bound forms of NCLX_Mj. In addition, the ion-coordinating residues at the S_{ext}, S_{mid}, S_{int}, and S_{Ca} sites of NCLX_M were mutated for testing the mutational effects on the ion-exchange activities with a goal of evaluating the ion binding/transport capacity and selectivity at respective sites.

2. Methods

2.1. Constructs and site-directed mutagenesis

DNA encoding wild-type NCX_Mj was amplified by PCR from a *Methanocaldococcus jannaschii* cDNA library (DSMZ) and ligated between the *Nco*I and *Bam*HI restriction sites of a pET-28a plasmid, as described before [23,27,29]. Single-point mutations were introduced by QuickChange mutagenesis (Stratagene) and were confirmed by sequencing, as previously outlined [22–25,31].

2.2. Isolation of E. coli-derived membrane vesicles overexpressing NCX_Mj, NCLX_Mj, and their mutants

Expression vectors were transformed into *E. coli* BL21 (DE3) pLysS competent cells [22,23,25]. *E. coli* cells were grown in 2xYT media with antibiotics. Protein expression was induced when cell cultures reached OD_{600} = 0.5–0.6 at 16 °C by adding 0.4 mM IPTG. After 12–16 h incubation, cells were harvested and resuspended in buffer containing 50 mM Mops-Tris pH 7.4, 0.25 M sucrose, 1 mM EDTA, 1 mM DTT, 100 Units/ml DNase, and 1 mM PMSF. The cells were disintegrated in a French press (at 20,000 psi) or in a Microfluidizer (at 14,000 psi) to obtain right side out (RSO) or inside out (ISO) vesicles, respectively [22,25,31]. The vesicles were isolated by using a three-step sucrose gradient (2.02, 1.4, and 0.7 M) at 150,000 × *g* for 15 h and the washed vesicles (in 50 mM Mops-Tris pH 7.4 and 0.25 M sucrose) were flash-frozen in liquid nitrogen and stored at −80 °C until use. The protein orientation in the *E. coli*-derived ISO and RSO vesicles was evaluated by using an antibody against the 6xHis-tag as reported before [22,23,25].

2.3. Ion-exchange assays using E. coli-derived vesicles or reconstituted proteoliposomes

Initial rates (t = 5 s) of Na^+/Ca^{2+}, Li^+/Ca^{2+}, and Ca^{2+}/Ca^{2+} exchange reactions were assayed at 35 °C by measuring the $^{45}Ca^{2+}$ uptake in *E. coli*-derived vesicles (containing the overexpressed protein) or in reconstituted proteoliposomes (containing the purified protein) [22,23,25,31]. The $^{45}Ca^{2+}$-uptake was initiated by a 25–200-fold dilution of vesicles loaded either with Na^+ (2–160 mM), Li^+ (2–160 mM), or Ca^{2+} (2–2000 μM) into a 0.2–0.5 ml assay medium (20 mM Bis-Tris propane, pH 6.5, and 160 mM KCl) with 2–2000 μM $^{45}CaCl_2$. The $^{45}Ca^{2+}$-uptake was quenched by rapid injection of cold EGTA-buffer

(5 ml) into the assay medium and the intravesicular $^{45}Ca^{2+}$ was measured by rapid filtration of the quenched solution through a GF/C filter [20,22,23,25,31]. Non-specific $^{45}Ca^{2+}$ signals (blanks) were measured and subtracted from the samples as a background (non-specific) signal [20,23,25]. GraFit 7.0 software (Erithacus Software, Ltd.) was used for fitting the experimentally obtained values of $^{45}Ca^{2+}$-uptake at varying ionic concentrations. The kinetic parameters were measured at least in three independent experiments and data are presented as mean ± SE. The k_{cat} values were calculated according to $k_{cat} = V_{max} / [E]_t$, where the V_{max} and $[E]_t$ values were experimentally derived as outlined before [22,23,25,31].

2.4. Overexpression and purification of NCX_Mj and NCLX_Mj proteins

The NCX_Mj and NCLX_Mj proteins or their mutants were overexpressed and purified according to previously described methods [20–25]. The proteins were purified from 200 to 400 g of *E. coli* cells. Briefly, the *E. coli* membranes, containing the overexpressed protein, were isolated from the cell lysate by ultracentrifugation at 200,000 ×*g* for 2 h and the cell membranes were stored at −80 °C until protein extraction. After extraction of membrane protein with 20 mM *n*-dodecyl-D-maltoside (DDM), insoluble material was removed by centrifugation and NCLX_Mj was purified from the supernatant using a Co^{2+} affinity column. The fraction eluted with 250 mM imidazole was desalted and then incubated overnight with TEV protease at 4 °C to cleave the His-tag. The cleaved protein was loaded again on a Co^{2+} column and the eluate was concentrated to 5–10 mg protein/ml [21–25]. The concentrated proteins were purified using a Superdex-200 column, which was pre-equilibrated with 0.5 mM DDM containing buffer [21,23,24]. Purified proteins (> 90% purity, as judged by SDS-PAGE) were concentrated, flash frozen, and stored at −80 °C until use.

2.5. Reconstitution of purified NCX_Mj and NCLX_Mj proteins into liposomes

Purified preparations of NCX_Mj and NCLX_Mj with 0.5 mM DDM buffer were reconstituted with a protein-to-lipid ratio of 1:100 (w/w) with POPE:POPG lipids (3:1). The detergent was removed by dialysis at 4 °C overnight and then incubated with SM-2 beads to ensure that all traces of detergent were removed [21]. After detergent removal, the reconstituted proteoliposomes were spun down and the pellet was dissolved in a minimal volume of buffer (20 mM MOPS, pH 6.5, and 50 mM CsCl). The reconstituted proteoliposomes were kept at −80 °C in 100–200 µL aliquots until use. Before the ion-flux assays, proteoliposomes were briefly sonicated in water-bath sonicator, yielding unilamellar vesicles. Then, the proteoliposomes were loaded with 100 mM NaCl or LiCl, 5 mM EGTA, 1 mM KCl at 35° C for 2 h. At 10–20 min prior to the ion-flux assay, the Na^+- or Li^+-loaded proteoliposomes were mixed with ± 2 µM valinomycin under vigorous vortexing. The reaction of Na^+- or Li^+-dependent $^{45}Ca^{2+}$uptake was initiated by a 100–200-fold dilution of NCX_Mj or NCLX_Mj containing proteoliposomes (preloaded with 160 mM NaCl or LiCl) into the assay medium with 20 mM Bis-Tris propane, pH 6.5, 160 mM KCl, and 100–500 µM $^{45}CaCl_2$. The reaction of $^{45}Ca^{2+}$-uptake was quenched at desired time points (5–250 s) by adding cold EGTA-containing buffer (see above). The quenched samples were rapidly filtered and dry filters were placed in scintillation vials to measure $^{45}Ca^{2+}$ content [20–23,31].

2.6. TMRM labeling of proteins

The purified proteins (see above) of single-cysteine mutants (NCLX_Mj-G42C or NCLX_Mj-G201C) were labeled according to protocols established for the cys-mutants of NCX_Mj [24]. Stock solutions of TMRM (50–500 µM) were prepared by dissolving TMRM in DMSO and the concentrations of stock solutions were calculated by measuring OD at 541 nm using an extinction coefficient of 95,000 cm − 1 M − 1 [32,33]. Purified preparations of cys-mutated proteins (0.2–0.3 mg/ml), kept in 0.5 mM DDM containing buffer, pH 7.1 (see above), were incubated with 0.5–1 µM TMRM at 4 °C for 0–240 min and the reaction of covalent labeling was terminated at indicated times by the rapid addition of cold DTT to a final concentration of 10 mM [24,32,33]. Quenched samples were subjected to SDS-PAGE analysis and gels were imaged using excitation and emission wavelengths of 540 and 595 nm, respectively [24,32,33]. The Fusion FX7 Spectra instrument (Vilber Lourmat™), equipped with "Fusion-Capture Advance" software, was used for quantitative evaluation of labeled protein bend density in each series of experiments. The normalized signals (for each gel run) were plotted *vs* time and the experimental points were fit to the first-order rate constants as previously reported [24].

2.7. Deuterium exchange for HDX-MS experiments

NCLX_Mj was prepared at 60 µM in the following buffers: a) 20 mM HEPES, pH 7.1, 100 mM Choline-Cl, 1% bicelle either with 2 mM EGTA or 2 mM $CaCl_2$; b) 20 mM HEPES, pH 7.1, 100 mM NaCl, 1% bicelle, 2 mM EGTA; c) 20 mM HEPES, pH 7.1, 100 mM LiCl, 1% bicelle, 2 mM EGTA. NCLX_Mj was reconstituted into bicelles by gentle mixing with bicelle stocks (3:1 M ratio of DMPC to CHAPSO) in a 1:9 ratio for 30 min to allow complete reconstitution. HDX was initiated by mixing 7 µL of the reconstituted protein with 23 µL of D_2O buffer. After incubation for 10, 100, 1,000, or 10,000 s at 4 °C, the samples were quenched with 30 µL of ice-cold quench buffer (100 mM NaH_2PO_4, pH 2.01). For non-deuterated samples (ND), 7 µL of reconstituted protein was mixed with 23 µL of H_2O buffer and quenched with 30 µL of ice-cold quench buffer. All data were derived from three independent experiments.

2.8. Mass spectrometry, peptide identification, and HDX data processing

The quenched samples were digested, and then analyzed using the HDX-UPLC-ESI-MS system (Waters, USA) as previously described [35]. Mass-spectral analyses were performed with an Xevo G2 Quadruple-time of fly (Q-TOF) equipped with a standard ESI source in MS^E mode (Waters, USA). The mass spectra were acquired in the range of *m/z* 100–2000 for 12 min in positive ion mode. Peptides were identified in non-deuterated samples with ProteinLynx Global Server (PLGS) 2.0 (Waters, USA). The following parameters were applied: monoisotopic mass, non-specific for the enzyme while allowing up to one missed cleavage, MS/MS ion searches, automatic fragment mass tolerance, and automatic peptide mass tolerance. Searches were performed with variable methionine oxidation modification, and the peptides were filtered with a peptide score of 6. To process the HDX-MS data, the deuterium amount in each peptide was determined by measuring the centroid of the isotopic distribution using DynamX 2.0 (Waters, USA). All data were derived from three independent experiments, and peptides with more than a 0.3-Da difference between the apo and ion-bound forms were considered different and further analyzed to derive the S.E.M. and tested with Student's *t*-test by using GraphPad Prism 5 (GraphPad Software).

3. Results

The primary goal of the present study was to evaluate the relative exposure of the cytosolic and extracellular vestibules of NCLX_Mj to the bulk phase under steady-state conditions. This is because the underlying structure-dynamic determinants may control the relative stability of the outward-facing (OF) and inward-facing (IF) states and thus, the intrinsic equilibrium (K_{int}) and rates (k_{cat}) of bidirectional ion movements in NCX and similar proteins [7,8,22]. Two independent approaches, previously established for NCX_Mj [22–24], were applied here for measuring K_{int} in NCLX_Mj (Fig. 1).

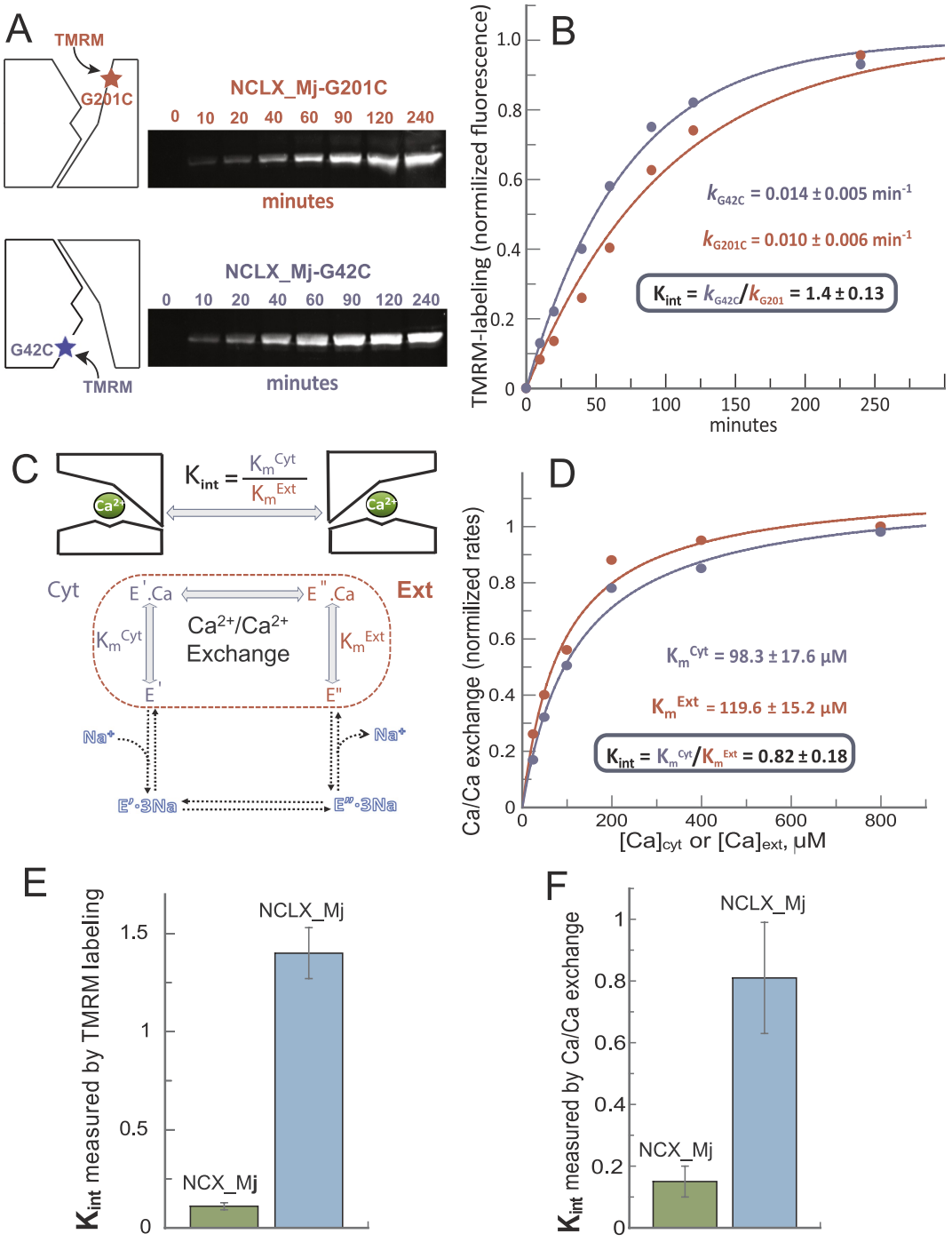

Fig. 2. The K_{int} values measured by TMRM-labeling and the Ca^{2+}/Ca^{2+} exchange assays. (A) Purified NCLX_Mj-G201C and NCLX_Mj-G42 proteins were incubated with 0.5 μM TMRM at 4 °C for 0–240 min and TMRM labeling was terminated by DTT at the indicated times. The TMRM-labeled bands were imaged for NCLX_Mj-G201C (upper panel) and for NCLX_Mj-G42C (lower panel) and the fluorescence signals were quantitated as outlined in Materials and Methods. (B) The quantitated in-gel fluorescence (panel A) signals were normalized and fit to mono-exponential curves with the time constants indicated. (C) The intrinsic equilibrium of bidirectional Ca^{2+} movements (K_{int}) is defined as the ratio of K_m^{Cyt} and K_m^{Ext} ($K_{int} = K_m^{Cyt}/K_m^{Ext}$) assayed for the Ca^{2+}/Ca^{2+} exchange. (D) The K_m^{Cyt} value was determined at varying $[Ca^{2+}]_{Cyt}$ (2–200 μM) and saturating $[Ca^{2+}]_{Ext}$ (2 mM). The K_m^{Ext} values was measured at varying $[Ca^{2+}]_{Ext}$ (10–2000 μM) and saturating $[Ca^{2+}]_{Cyt}$ (2 mM). (E) Comparison of the K_{int} values measured for NCX_Mj and NCLX_Mj by using the TMRM-labeling assay. (F) Comparison of the K_{int} values measured for NCX_Mj and NCLX_Mj by using the Ca^{2+}/Ca^{2+} exchange assays. Bars represent the mean ± SE values.

3.1. Measurement of K_{int} by TMRM-labeling of the cytosolic and extracellular vestibules

In the first approach (Fig. 2A,B), the accessibility of the cytosolic and extracellular vestibules to the bulk phase was measured by labeling the purified preparations of the single-cysteine mutants of NCLX_Mj with fluorescent TMRM (tetramethylrhodamine-5-maleimide), as previously reported for NCX_Mj [24]. Notably, NCLX_Mj (alike to NCX_Mj) contains two endogenous cysteine residues (C78 and C80), but they do not interfere with the TMRM assay, since these cysteine residues are deeply buried in the core of the folded protein and thus, they are inaccessible to bulk-phase TMRM. In the present experimental setup, solvent accessibility to the intracellular and extracellular vestibules of NCLX_Mj to the bulk phase was measured as time-dependent

labeling of purified apo NCLX_Mj-G42C (cytosolic vestibule) and apo NCLX_Mj-G201C (extracellular vestibule) with TMRM (Fig. 2A,B). Comparable rates of TMRM labeling were observed for NCLX_Mj-G42C (k_{G42C} = 0.014 ± 0.005 min^{-1}) and NCLX_Mj-G201C (k_{G201C} = 0.010 ± 0.006 min^{-1}), revealing a K_{int} value of 1.4 ± 0.2 (Fig. 2B). These results are consistent with a nearly equal exposure of the cytosolic and extracellular vestibules to the bulk phase, meaning that the open IF and OF states are comparably stabilized in apo-NCLX_Mj. This "symmetric" mode of bidirectional exposure in apo-NCLX_Mj strikingly differs from apo-NCX_Mj, showing a preferential stabilization of the OF state with K_{int} of 0.1 ± 0.03 (Fig. 2E).

3.2. Measurement of K_{int} using the Ca^{2+}/Ca^{2+} exchange assay

In the second experimental approach (Fig. 2C), the intrinsic equilibrium (K_{int}) for bidirectional ion movements was measured by assaying the Ca^{2+}/Ca^{2+} exchange rates in membrane vesicles containing uniformly oriented (overexpressed) protein [22,23]. In this assay system, the K_{int} values of Ca^{2+} bidirectional movements ($K_{int} = K_m^{Cyt}/K_m^{Ext}$) were derived for NCLX_Mj by measuring the K_m^{Cyt} and K_m^{Ext} values by using the protocols established for NCX_Mj [22,23]. In these experiments, the initial rates (t = 5 s) of Ca^{2+}/Ca^{2+} exchange were measured at varying $[Ca^{2+}]_{Cyt}$ and saturating $[Ca^{2+}]_{Ext}$ values for evaluating the K_m^{Cyt} values. In parallel experiments, the K_m^{Ext} values were measured by assaying the initial rates of Ca^{2+}/Ca^{2+} exchange at varying $[Ca^{2+}]_{Ext}$ and saturating $[Ca^{2+}]_{Cyt}$ values (Fig. 2C,D). The measured values of K_m^{Cyt} = 98.3 ± 17.6 μM and K_m^{Ext} = 119.6 ± 15.2 μM revealed a K_{int} value of 0.82 ± 0.18 (Fig. 2D). Thus, the K_{int} values of NCLX_Mj, measured by using the TMRM-labeling (Fig. 2A,B) and Ca^{2+}/Ca^{2+} exchange assays (Fig. 2C,D), are comparable (K_{int} = 0.8–1.4), thereby revealing that the intrinsic equilibrium of bidirectional exposure approaches unity ($K_{int} \simeq 1$). These data represent the "symmetric" accessibility of the extracellular and cytosolic vestibules in NCLX_Mj. Notably, the K_{int} values of NCX_Mj are at least 8–15 times lower than the K_{int} values of NCLX_Mj, while the K_{int} measurements were done by using the TMRM-labeling (Fig. 2E) or the Ca^{2+}/Ca^{2+} exchange (Fig. 2F) protocol. Thus, the two independent approaches produce consistent values of K_{int} either for NCLX_Mj or NCX_Mj.

3.3. Apo-NCLX_Mj exhibits characteristic profiles of backbone dynamics

The functional asymmetry ($K_{int} < 1$) in NCX_Mj is associated with the conformational "asymmetry" of backbone dynamics at specific segments involved in ion binding, occlusion, and translocation [23,24,37]. Given the characteristic features of NCLX_Mj, including the ion-selectivity profiles and the capacity for "symmetric" exposure of the cytosolic and extracellular vestibules, we sought to characterize the backbone dynamics of apo-NCLX_Mj. For this purpose, purified apo-NCLX_Mj was analyzed by HDX-MS (Fig. 3), as was previously done with apo-NCX_Mj [23,24]. The overall sequence coverage (29.2%) of NCLX_Mj (Fig. S1) is similar to that of NCX_Mj. Although the sequence coverage is low, the identified peptides cover 10 out of 12 ion-coordinating residues located on 3 out of 4 TMs (TM2, TM7, and TM8 but not TM3) (Figs. 1 and S1).

The HDX profile of apo-NCLX_Mj is overlaid on the crystal structure of NCX_Mj as heat maps after a 10 and 10,000 s deuterium exchange (Fig. 3A). The deuterium uptake plot of each peptide is shown in Fig. S2. As expected, the solvent-exposed ion-coordinating regions at TM2, TM7, and TM8 exhibit higher deuterium uptake, compared with the core region of the membrane-embedded TM (e.g., at TM6). The middle of TM8 exhibits higher HDX levels than the other regions do, suggesting that this region is more dynamic or more exposed to the bulk phase, compared with other ion-coordinating TMs (Fig. 3). This dynamic profile is similar to that observed before in NCX_Mj [23,24]. Interestingly, in NCLX_Mj the counterpart peptides 47–56 (TM2) and 205–214 (TM7), representing matching positions in the inverted twofold "pseudo-symmetry", exhibit similar HDX rates, with TM7 having slightly higher deuterium uptake rates (Fig. 3B). Previous analysis of NCX_Mj revealed that these regions exhibit markedly asymmetric conformational dynamics despite their symmetrical positions and sequences, with peptide 47–56 having a much lower HDX level than peptide 205–214 [24] (Fig. 7B, left). In contrast with NCX_Mj, comparable levels of deuterium uptake in peptides 47–56 and 205–214 are correlated with reduced HDX at TM2 of NCLX_Mj (rather than with enhanced HDX at TM7)(Fig. 7B, right). Thus, in line with the TMRM-labeling assay and Ca^{2+}/Ca^{2+} assays (Fig. 2), the similar backbone dynamics of inversely matched positions (located at the cytosolic and extracellular vestibules) reveal a rather symmetric structure-dynamic preorganization of apo-NCLX_Mj. Interestingly, these results differ from those of NCX_Mj, where the HDX-MS and TMRM-labeling analyses reveal the predominant stabilization of the OF state [24]. Thus, accumulating data motivated us to test the effects of ions on the conformational dynamics of NCLX_Mj, with the goal of determining how the binding of Na^+, Li^+, or Ca^{2+} alters the local backbone dynamics at distinct sites of NCLX_Mj.

3.4. Effects of ion binding on the NCLX_Mj backbone dynamics

The ion binding sites of NCLX_Mj are extensively modified compared with those of NCX_Mj and can accommodate either Na^+ or Li^+ ions. Therefore, we sought to characterize the binding of the different transported ions by NCLX_Mj with HDX-MS. The difference in HDX upon ligand binding is qualitatively illustrated on the crystal structure of NCX_Mj as reduced HDX (blue) or increased HDX (red) (Fig. 4). The uptake plots for each peptide are shown in Fig. S2. Overall, the addition of saturating concentrations of Ca^{2+} (2 mM), Na^+ (100 mM), or Li^+ (100 mM) reduces the HDX rates in NCLX_Mj. All tested ions have no effect on the HDX profiles of the peptides from the TM6 and TM6/TM7 loop (Fig. 4 and S2, peptides 175–182 and 193–199), which obviously do not participate in ion binding. In contrast, each ion differentially affected the conformational dynamics of the ion-coordinating TMs of NCLX_Mj (Figs. 4 and S2).

Both Na^+- and Li^+-binding result in reduced deuterium uptake within peptides 47–56 (TM2B, encompassing A47, N50, G51, and D54 from sites S_{int} and S_{Ca}) and 216–230 (TM7C) and increased deuterium uptake within peptide 227–233 (TM8A) (Fig. 4A and B, Fig. S2). However, only Li^+-binding reduces deuterium uptake within peptide 248–255 (TM8C) (Figs. 4B, S2). Moreover, Ca^{2+} binding results in reduced deuterium uptake within peptides 47–56 (TM2B, encompassing A47, N50, G51, and D54 from sites S_{int} and S_{Ca}), 216–230 (TM7C), and 238–245 (the middle of TM8, encompassing N240 from S_{mid}), without having any additional appreciable effects at the S_{ext} and S_{int} sites (Figs. 4C and S2). Notably, the residues belonging to the S_{ext} site (A206, N209, and S210) were not affected by any ion. Moreover, the binding of either the Na^+ or Ca^{2+} ions to NCX_Mj results in much more dispersed and stabilized (rigidified) TM2, TM7, and TM8 [23,24], compared with the ion-induced effects observed for NCLX_Mj (Figs. 4 and S2).

3.5. The effect of voltage clamp on the NCLX-mediated ion-exchange rates

Previous measurements of Na^+/Ca^{2+} and Li^+/Ca^{2+} exchange rates (by using uniformly oriented vesicles) revealed comparable values of K_m^{Cyt}(Ca) for Na^+/Ca^{2+} and Li^+/Ca^{2+} exchange reactions mediated by NCX_Mj or NCLX_Mj [31]. By using the same experimental protocols, we determined the K_m^{Ext}(Na) values for NCX_Mj and NCLX_Mj. The K_m^{Ext}(Na) values are at least 20–30-times lower in NCLX_Mj compared to the K_m^{Ext}(Na) of 18 ± 2.6 mM observed for NCX_Mj (Fig. 5A,B). In contrast with this, both proteins have similar values of K_m^{Ext}(Ca) = 125–180 μM for the Na^+/Ca^{2+} and Li^+/Ca^{2+} exchange reactions (Fig. 5C). Moreover, the K_m^{Ext}(Na) and K_m^{Ext}(Li) values are nearly identical for NCLX-mediated Na^+/Ca^{2+} and Li^+/Ca^{2+} exchange

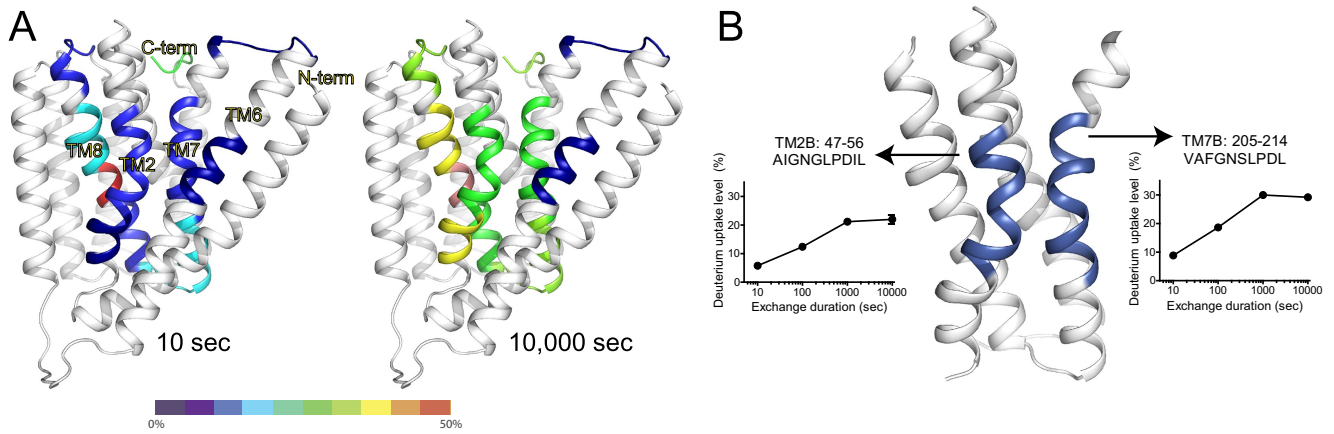

Fig. 3. HDX-MS of apo-NCLX_Mj. The HDX-MS analysis of purified NCLX_Mj (60 μM) was performed in the absence of the Na^+, Li^+, or Ca^{2+} ions by using the buffer containing 2 mM EGTA, as described in Materials and Methods. **(A)** Heat maps for NCLX_Mj at 10 s (left) and 10,000 s (right) of the deuterium exchange are overlaid on the crystal structure of NCX_Mj. **(B)** Close-up view of TMs 2,3,7, and 8. The residues in blue correspond to peptides, as shown in the associated uptake plots.

reactions, thereby underscoring hallmark differences between NCX_Mj and NCLX_Mj (Fig. 5A,B). These data, in conjunction with the HDX-MS data described above, suggest a possibility that the ion-exchange stoichiometry could be different in NCX_Mj and NCLX_Mj. To further investigate this possibility, we tested the response of the Na^+/Ca^{2+} or Li^+/Ca^{2+} exchange rates to voltage clamping in reconstituted proteoliposomes containing the purified NCX_Mj or NCLX_Mj proteins. This analysis was based on the assumption that the clamping of positive inside potential (managed by valinomycin/KCl) must accelerate the electrogenic ion-exchange ($3Na^+:1Ca^{2+}$). In these experiments the initial rates of Na_i^+- or Li_i^+-dependent $^{45}Ca^{2+}$-uptake were measured at saturating concentrations of ions at both sides of the membrane by using the valinomycin-treated (positive inside) and untreated (zero potential) proteoliposomes (Fig. 5D). Notably, the positive inside potential accelerates the initial rates of Na_i^+-dependent $^{45}Ca^{2+}$-uptake in NCX_Mj-reconstituted proteoliposomes (as is expected for electrogenic ion-exchange), whereas there is no indication for acceleration of Na_i^+- or Li_i^+-dependent $^{45}Ca^{2+}$-uptake in NCLX_Mj-reconstituted proteoliposomes upon clamping the positive inside potential (Fig. 5D). According to these data, either the NCLX_Mj mediated ion-exchange is electroneutral (e.g., $2Na^+:1Ca^{2+}$ or $2Li^+:1Ca^{2+}$) or alternatively, the electrogenic transport step (e.g., the translocation of $3Na^+$ or $3Li^+$) is not rate-limiting along the transport cycle. The experimental resolution between these two possibilities does not seem to be trivial.

3.6. Mutational analysis for evaluating the functional status of ion-binding sites in NCLX_Mj

Given the characteristic HDX profiles observed at the ion binding helices of NCLX_Mj (see above), we sought to evaluate the functional status of distinct ion-binding sites in NCLX_Mj by testing the effects of site-directed mutagenesis on the transport activities. In these experiments the V_{max}, K_m(Na), K_m(Li) and K_m(Ca) values of Na^+/Ca^{2+} and Li^+/Ca^{2+} exchange reactions were measured by using the uniformly oriented *E. coli* membrane vesicles (see Materials and Methods) containing the overexpressed mutants of NCLX_Mj (Fig. 6). Nine residues of NCLX_Mj, out of twelve (selected according to the matching positions of ion-coordinating residues in NCX_Mj), were tested for their mutational effects on the ion-transport activities with the goal of evaluating the functional assignments of four binding sites (S_{ext}, S_{int}, S_{mid} and S_{Ca}) in NCLX_Mj. The single-point mutations of D54 (S_{ext}, S_{mid} and S_{Ca}), D213 (S_{int}, S_{mid} and S_{Ca}) and N240 (S_{mid}) have a devastating effect on both the Na^+/Ca^{2+} and Li^+/Ca^{2+} exchange activities, thereby underscoring the essential role of these residues in controlling the ion-transport activities in NCLX_Mj (Fig. 6A). Notably, the matching three residues in NCX_Mj (E54, E213 and D240) are also functionally important [23]. However, the mutations of six residues (N50, G51, A77, N209, S210 and G236) have different effects on the V_{max} values of NCLX_Mj-mediated ion-fluxes (Fig. 6B) as compared with NCX_Mj [23], meaning

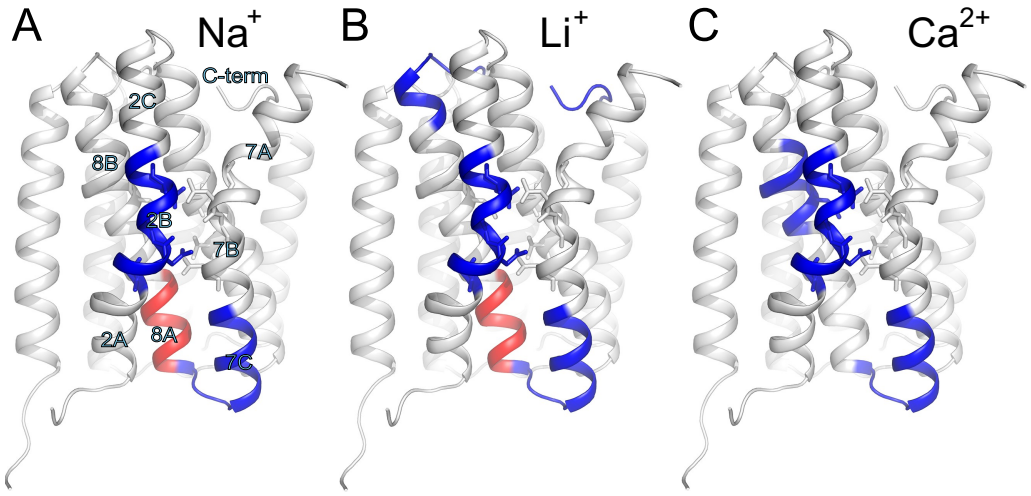

Fig. 4. Effect of ion binding on the HDX of NCLX_Mj. For evaluating the ion-dependent changes in HDX, the purified preparations of NCLX_Mj were analyzed in the presence of 100 mM Na^+ + 2 mM EGTA (A), 100 mM Li^+ + 2 mM EGTA (B), or 2 mM Ca^{2+} as described in Materials and Methods (C). The ion-dependent changes in the backbone dynamics are shown by aligning the HDX data on the crystal structure of NCX_Mj (PDB 3V5U). Regions labeled in blue show reduced HDX, whereas regions labeled in red show increased HDX.

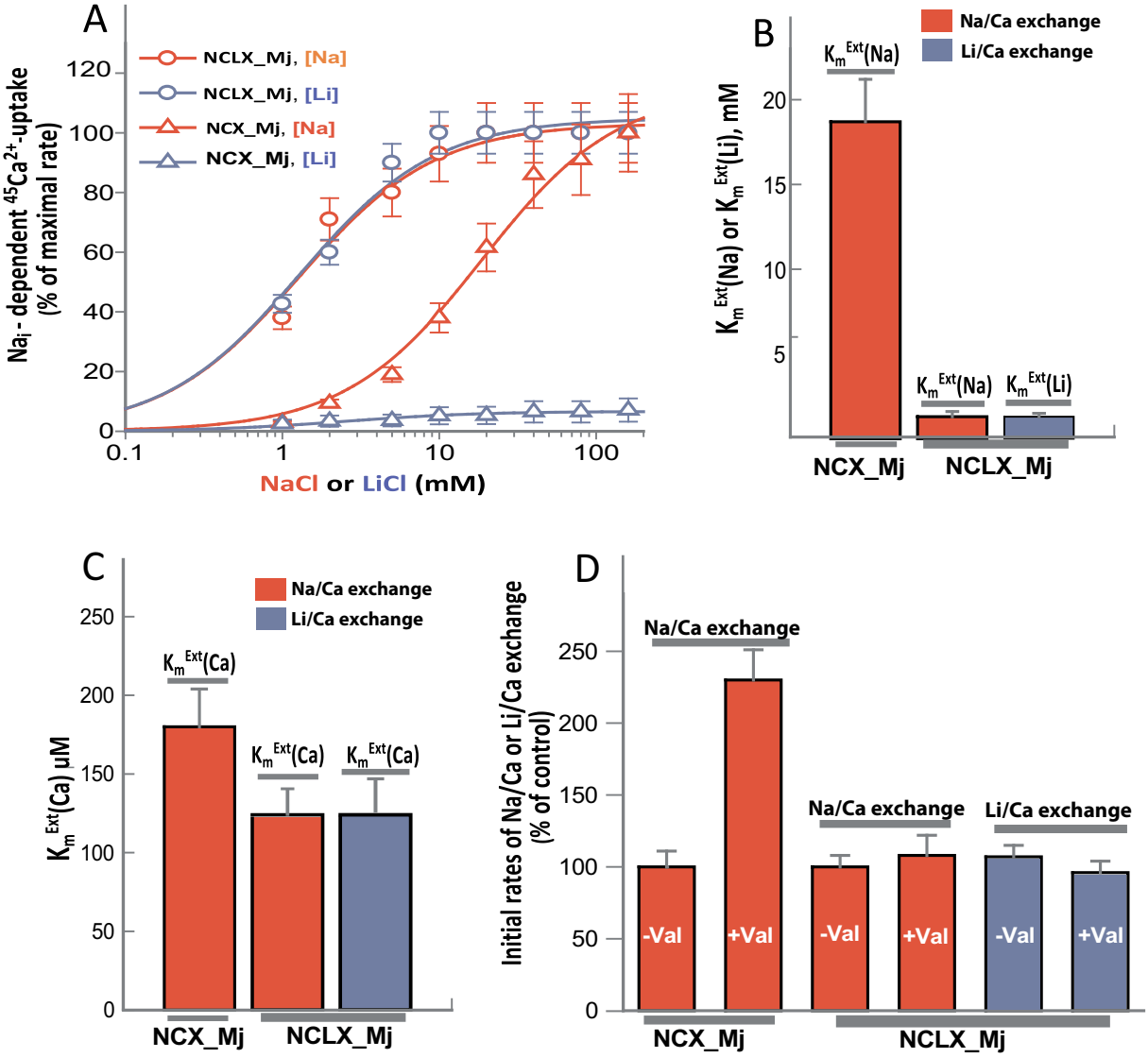

Fig. 5. Comparison of NCLX_Mj- and NCX_Mj-mediated ion exchange properties. (A) The $[Na^+]$- and $[Li^+]$-dependent $^{45}Ca^{2+}$ uptake was measured by diluting the Na^+- or Li^+-loaded *E. coli* vesicles containing the overexpressed NCLX_Mj or NCX_Mj proteins into the assay medium containing 200 µM $^{45}Ca^{2+}$ (for details, see Materials and Methods). The experimental points were normalized according to maximal signals obtained at saturating Na^+ or Li^+, respectively. The fitted lines represent the K_m^{Ext}(Na) = 0.35 ± 0.1 mM and K_m^{Ext}(Li) = 0.39 ± 0.1 mM values for NCLX_Mj and the K_m^{Ext}(Na) = 18 ± 2.6 mM value for NCX_Mj. (B) The K_m^{Ext}(Na) and K_m^{Ext}(Li) values were derived from the measurements described in panel A. Bars represent the mean ± SE. **(C)** The K_m^{Ext}(Ca) values were derived for the Na^+/Ca^{2+} or Li^+/Ca^{2+} exchange reactions by diluting the Na^+ (160 mM) or Li^+ (160 mM) loaded vesicles into the assay medium containing 10–2000 µM $^{45}Ca^{2+}$. Bars represent the mean ± SE. (D) The effect of the voltage clamp (managed by the valinomycin/KCl system) was tested on the ion-exchange rates by using the reconstituted preparations of proteoliposomes containing purified NCX_Mj or NCLX_Mj (for details, see Materials and Methods). Briefly, Na^+ (100 mM) or Li^+ (100 mM)-loaded vesicles (± valinomycin) were diluted (at 35 °C) in the assay medium containing 50 µM $^{45}Ca^{2+}$ and 100 mM KCl. The initial rates of $^{45}Ca^{2+}$ uptake were measured by quenching the reaction with rapid injection of cold EGTA-containing buffer. Bars represent the mean ± SE (n = 7).

that different residues might be involved in NCLX_Mj-mediated transport of Na^+ or Li^+ in comparison with the Na^+ transport through NCX_Mj. The mutation of N50, A77, N209 or S210 increase 5–10-fold the K_m for Na^+ or Li^+ (Fig. 6B,C), indicating that these residues could be involved in the ground state (but not the transition state) binding of Na^+ or Li^+ ions. Collectively, the present mutational analysis reveals that the Ca^{2+}, Na^+ or Li^+ ions can interact with the S_{Ca} site of NCLX_Mj, whereas the functional assignments of the "Na^+-sites" (S_{ext}, and S_{int}) are not identical in NCLX_Mj and NCX_Mj. Although the present analysis cannot identify carbonyl group(s) involved in the coordination of Na^+ or Li^+, the relevant modes of ion-ligation could be also different in NCLX_Mj and NCX_Mj. Thus, the crystal structure of NCLX_Mj is required for disclosing the structural organization of ion binding sites in NCLX_Mj.

4. Discussion

4.1. NCLX_Mj exhibits a comparable accessibility to ions at opposite sides of the membrane

Despite 10^4-fold differences in the transport cycle turnover rates, the plasma-membrane NCXs of eukaryotic and prokaryotic species share a functional asymmetry in bidirectional ion movements [3,7–9,22–24,37]. The previous studies using TMRM-labeling, HDX-MS and Ca^{2+}/Ca^{2+} exchange assays, have shown that in the presence or absence of ions the NCX_Mj protein preferentially adopts the extracellular (OF) orientation with $K_{int} \leq 0.15$ [22–24]. These findings are consistent with the determined crystal structures of the open, semi-open and occluded states of NCX_Mj, which all adopt the OF orientation

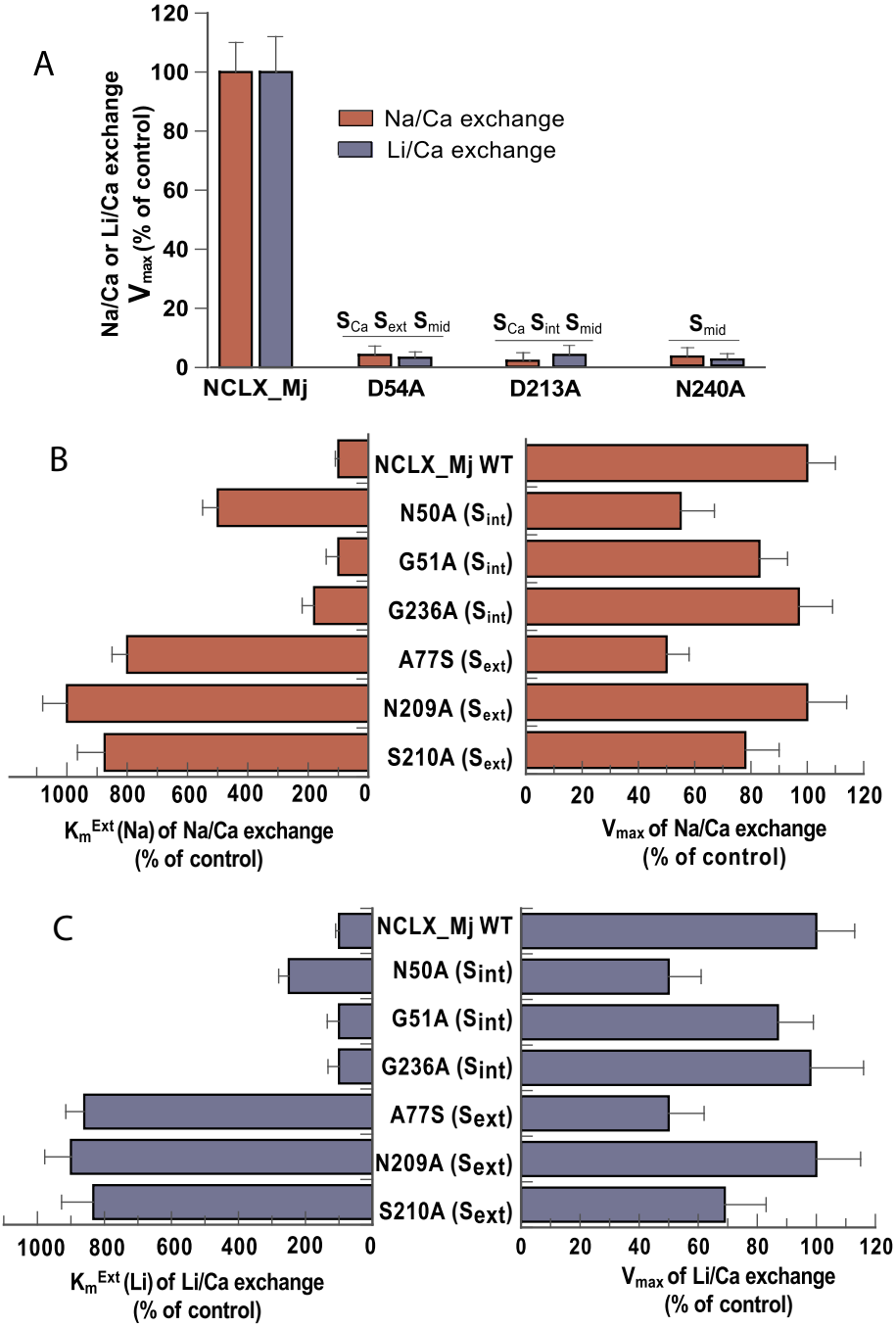

Fig. 6. Mutational effects on NCLX-mediated Na^+/Ca^{2+} and Li^+/Ca^{2+} exchange activities. The $[Na^+]$- and $[Li^+]$-dependent $^{45}Ca^{2+}$-uptake were measured by diluting the Na^+- or Li^+-loaded *E. coli* vesicles containing overexpressed NCLX_Mj in an assay medium containing saturating concentrations of $^{45}Ca^{2+}$ (200 μM) as described in Materials and Methods and Fig. 5. The K_m^{Ext}(Na) and K_m^{Ext}(Li) values were measured by fitting the experimental points with calculated lines (for details see the legend of panels A and B in Fig. 5).

[21,26]. Recent HDX-MS studies have shown that the structure-functional asymmetry in NCX_Mj is associated with signature profiles of the local backbone dynamics at specific segments of ion-coordinating helices [23,24]. Moreover, the characteristic profiles of conformational and functional asymmetry are largely predefined by specific structural elements of apo-NCX_Mj [7–9,23,24,56]. Here, the TMRM-labeling and Ca^{2+}/Ca^{2+} exchange measurements revealed the K_{int} values of 0.8–1.4 (Fig. 2A–D) for NCLX_Mj, which are at least 10-times higher than the K_{int} values measured for NCX_Mj under identical conditions (Fig. 2E,F). These functional features of NCLX_Mj are consistent with symmetric rigidity of apo- and ion-bound species of NCLX_Mj, detected by HDX-MS (Figs. 3 and 4). Thus, in contrast with NCX_Mj, the counterpart vestibules of NCLX_Mj are comparably (symmetrically) accessible for ions from the opposite sides of the membrane (Fig. 7A). These distinct abilities of the NCX_Mj and NCLX_Mj proteins to expose the extracellular and cytosolic vestibules to the bulk phase may represent the differential stabilities of the IF and OF states, where the degree of intrinsic asymmetry is predefined by structural specificities of a given apo-protein.

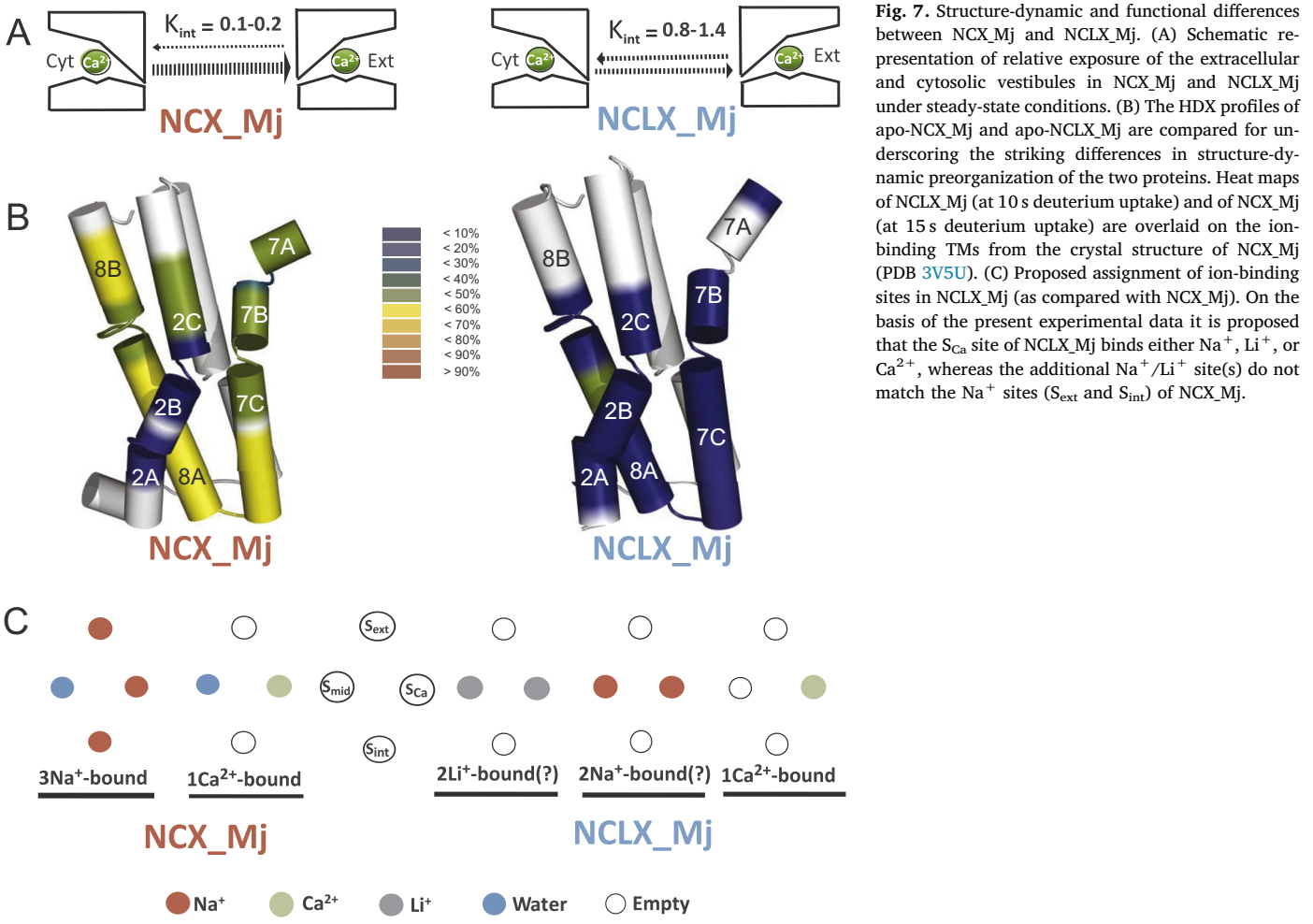

Fig. 7. Structure-dynamic and functional differences between NCX_Mj and NCLX_Mj. (A) Schematic representation of relative exposure of the extracellular and cytosolic vestibules in NCX_Mj and NCLX_Mj under steady-state conditions. (B) The HDX profiles of apo-NCX_Mj and apo-NCLX_Mj are compared for underscoring the striking differences in structure-dynamic preorganization of the two proteins. Heat maps of NCLX_Mj (at 10 s deuterium uptake) and of NCX_Mj (at 15 s deuterium uptake) are overlaid on the ion-binding TMs from the crystal structure of NCX_Mj (PDB 3V5U). (C) Proposed assignment of ion-binding sites in NCLX_Mj (as compared with NCX_Mj). On the basis of the present experimental data it is proposed that the S_{Ca} site of NCLX_Mj binds either Na^+, Li^+, or Ca^{2+}, whereas the additional Na^+/Li^+ site(s) do not match the Na^+ sites (S_{ext} and S_{int}) of NCX_Mj.

4.2. Ion-coordinating helices of apo-NCLX_Mj exhibit characteristic backbone dynamics

Previous analysis of NCX_Mj by HDX-MS has shown that TM2B is intensely rigid in face of flexible TM2C, TM7B, TM7C, and TM8AB in apo-NCX_Mj, thereby describing a conformational asymmetry of ion-coordinating helices in the absence of ions [23,24]. The present HDX-MS analysis of apo-NCLX_Mj reveals rather symmetric conformational constraints at TM2B and TM7B in the middle of the ion-binding pocket, whereas the neighboring ion-coordinating TM segments are more flexible (Fig. 3). Thus, the conformational dynamics of apo-NCLX_Mj strikingly differ from those of apo-NCX_Mj, where the rigid TM2B faces more flexible TMs, hence allowing a higher degree of freedom for ion coordination [23,24]. Thus, the replacement of nine ion-coordinating residues in NCX_Mj results in a more rigid and symmetric core (TM2B/TM7B) in NCLX_Mj (Fig. 3), which in turn, can precondition the ion interactions with respective sites of NCLX_Mj. In any case, the observed dynamic symmetry of the rigid TM2B/TM7B core is associated with the unity values of K_{int} in NCLX_Mj (Fig. 2). In contrast with NCLX_Mj, the ion-coordinating helices are asymmetrically rigidified in NCX_Mj [24,56], while showing at least 10–20-fold lower values of K_{int} compared with NCLX_Mj (Fig. 2E,F). In general, the observed conformational differences between the NCX_Mj and NCLX_Mj proteins (Fig. 7B) are consistent with the notion that there are dramatic differences in the structure-dynamic organization of ion binding sites in NCX_Mj and NCLX_Mj, which affect not only the ion selectivity and the relative stability of the IF and OF states but also shape physiologically relevant parameters (transport rates, stoichiometry, K_m values, response to membrane potential, and more). Thus, the HDX-MS analysis was further explored to elucidate the ion-induced conformational changes at distinct ion-binding sites (see below).

4.3. Ion-induced conformational changes dramatically differ in NCLX_Mj and NCX_Mj

In NCLX_Mj, Li^+ or Na^+ induce similar HDX changes, whereas both ions rigidify TM2B and TM7C, with concomitant enhancement of TM8A flexibility (Fig. 4). Similar to Na^+ or Li^+, Ca^{2+} rigidifies TM2B and TM7C. However, in addition to these effects, Ca^{2+} also rigidifies TM8B, which is not affected by either Na^+ or Li^+ (Fig. 4). Thus, the binding of Na^+, Li^+, and Ca^{2+} to NCLX_Mj rigidifies TM2B and TM7C, whereas the Na^+ or Li^+ ions enhance TM8A flexibility (not observed for Ca^{2+}). Collectively, the Na^+, Li^+, and Ca^{2+}-dependent rigidification of TM2B and TM7C represents the interaction of these ions with the S_{Ca} site of NCLX_Mj. Notably, the effects of Ca^{2+} on TM2B and TM8 are more pronounced than the effects induced by Na^+ or Li^+ at the same locations (Figs. 4 and S2). The signature effects of Ca^{2+} can be explained by stronger binding of Ca^{2+} *vs* Na^+ or Li^+ at S_{Ca}. Moreover, strong binding of Ca^{2+} to S_{Ca} may represent a different accessibility of water at the S_{mid} site of NCLX_Mj and NCX_Mj [14,25,26]. This can be explained by the D → N replacement at position 240 in NCLX_Mj [25,31]. Although HDX-MS displays hallmark changes in the local backbone dynamics upon ion interactions with S_{Ca}, there is no indication of ion-induced changes in HDX at S_{ext} (Fig. 4). Moreover, the ion-induced HDX signals only partially cover the S_{mid} and S_{int} regions. In contrast with these observations, the hallmark changes in the backbone dynamics of NCX_Mj were observed upon Na^+ binding to the S_{ext}, S_{Ca}, and S_{int} sites [24]. Thus, the available data support the notion that the S_{Ca} site plays

a similar role in NCLX_Mj and NCX_Mj [24–26,56], even though all four residues contributing to the Ca^{2+}, Na^+ or Li^+ ligation at S_{Ca}, are different in NCLX_Mj and NCX_Mj (Fig. 1). In contrary, the assignment of the monovalent ion binding-sites (corresponding to S_{ext} and S_{int}) seems to be incompatible in NCX_Mj and NCLX_Mj. This conclusion was further confirmed by mutational studies (see below).

4.4. What is the stoichiometry of the Na^+/Ca^{2+} or Li^+/Ca^{2+} exchange in NCLX_Mj?

The present analysis has demonstrated that the voltage-clamp (controlled by the valynomycin/KCl system) accelerates the initial rates of the Na^+/Ca^{2+} exchange rates (as expected for an electrogenic system with a stoichiometry of $3Na^+:1Ca^{2+}$) in proteoliposomes containing the purified preparations of reconstituted NCX_Mj (Fig. 5D). In contrast with NCX_Mj, the initial rates of the Na^+/Ca^{2+} or Li^+/Ca^{2+} exchange are insensitive to voltage clamp, while using the same experimental system with the purified preparations of NCLX_Mj reconstituted into proteoliposomes (Fig. 5D). Although these data suggest the electroneutral mode of ion-exchange in NCLX_Mj (e.g., $2Na^+$:1Ca or $2Li^+:1Ca^{2+}$), a precaution must be taken knowing that the voltage-sensitive ion-exchange rates can be detected only if the electrogenic step of the transport cycle (e.g., the translocation of $3Na^+$) is rate limiting. Previous studies, with mammalian NCX systems, have shown that the translocation of $3Na^+$ is the electrogenic and rate-limiting step along the transport cycle [38–42]. This conclusion seems to be valid for NCX_Mj as well, since this protein is sensitive to the voltage-clamp (Fig. 5D). Given the present results, two alternative possibilities must be considered for NCLX_Mj. The first possibility is that NCLX_Mj mediates an electrogenic stoichiometry of ion-exchange (like NCX_Mj), where the rate-limiting step is electroneutral. The second possibility is that NCX_Mj mediates an electroneutral stoichiometry of ion exchange regardless of the features assigned to the rate-limiting step. Although the present studies cannot distinguish between these possibilities, the second possibility seems to be more consistent with mutational studies (see below). More dedicated experimental approaches are required for elucidating the stoichiometry of ion exchange modes in NCLX_Mj.

4.5. Mutational studies reveal that the Na^+/Li^+ sites are incompatible in NCLX_Mj and NCX_Mj

Among the nine matching residues replaced in NCLX_Mj (Fig. 1), the side-chains of five residues (T50 N, E54D, T209 N, E213D, and D240N) can potentially coordinate ions, whereas the side-chains of the other four residues (S51G, S77A, N81 V, and S236G) lack ion-coordinating capacity. For evaluating the functional capacities of individual residues at assigned sites, nine residues of NCLX_Mj were mutated and tested for their effects on the Na^+/Ca^{2+} or Li^+/Ca^{2+} exchange activities (Fig. 6). The mutations of D54 (S_{ext}, S_{mid}, and S_{Ca}), D213 (S_{int}, S_{mid} and S_{Ca}), or N240 (S_{mid}) dramatically decrease NCLX_Mj-mediated ion-transport activities (Fig. 6A). However, the mutation of N50, G51, A77, N209, S210, or G236 (exclusively assigned to S_{ext} and S_{int}) in NCLX_Mj do not appreciably alter (if at all) the V_{max} values of either the Na^+/Ca^{2+} or Li^+/Ca^{2+} exchange (Fig. 6B,C). Moreover, these mutations do not alter the K_m value of Ca^{2+} (Fig. S3). Interestingly, the mutation of N50, A77, N209, or S210 increase 5–10-fold the K_m value for Na^+ or Li^+ (Fig. 6B,C), meaning that these residues could be involved in Na^+ or Li^+ binding. Collectively, the present findings reveal that the S_{Ca} site of NCLX_Mj can bind/transport either the Ca^{2+}, Na^+ or Li^+ ions, whereas the structural assembly of additional Na^+ (or Li^+) binding site(s) strictly differ in NCLX_Mj and NCX_Mj. Thus, the Na^+-coordinating residues at S_{ext} and S_{int} of NCX_Mj are not compatible with the matching residues of NCLX_Mj. This definition is in line with the experimental fact that the K_m values of Na^+ (or Li^+) are at least 10–20-fold lower in NCLX_Mj than in NCX_Mj (Fig. 5A,B), whereas the K_m values of Ca^{2+} are comparable for both proteins (Fig. 5C). These findings are also consistent with the HDX-MS data demonstrating that S_{Ca} of NCLX_Mj can bind Ca^{2+}, Na^+ or Li^+, whereas there is no evidence for interaction of these ions with the S_{ext} and S_{int} sites (see above). The present study cannot either confirm or exclude the Na^+ (or Li^+) binding to S_{mid} of NCLX_Mj, although the occupation of the S_{mid} site either by Na^+ or Li^+ would be compatible with "symmetric" conformational organization of NCLX_Mj (Fig. 7B).

4.6. Possible physiological relevance of the structure-functional determinants of NCLX_Mj

Several lines of evidence suggest that NCX_Mj can bind $3Na^+$ ions without occupying the S_{mid} site [23–26], whereas in NCKX (exhibiting the stoichiometry of $4Na^+:1Ca^{2+},1\ K^+$) the S_{mid} site can be occupied either by Na^+ or K^+ [5,6,14,43]. No matter how the binding sites are structurally organized (or assigned) in NCLX_Mj, it seems highly improbable that NCLX_Mj binds 3 Na^+ (or $3Li^+$) ions (Fig. 7C). In any case, the present findings underscore the structure-dynamic and functional differences in ion interactions between NCX_Mj and NCLX_Mj, which may have physiological relevance for intact NCLX proteins. More specifically, the underlying mechanisms may control the physiologically relevant features of bidirectional ion movements (ion selectivity, K_m values, ion-transport stoichiometry, response to membrane potential changes, and the directionality of Ca^{2+} entry/extrusion modes, among others). Thus, the unique arrangements of ion-coordinating residues in NCLX_Mj (and perhaps in native NCLX as well) may specifically govern the differential contributions of NCX [7–9,44–47] and NCLX [4,16,48–50] to Ca^{2+} signaling in distinct subdomains [18,49,50]. These structure-dynamic and functional relationships are especially interesting in light of the fact that the NCX and NCLX proteins have to respond to and integrate the cytosolic and mitochondrial Ca^{2+} homeostasis at distinct subcellular domains [16,49,50]. For example, the Ca^{2+}-dependent allosteric regulation of mammalian NCX and mitochondrial NCLX are fundamentally different, since the cell-membrane NCXs contain the Ca^{2+}-binding regulatory domains (CBD1 and CBD2), whereas NCLX completely lacks these regulatory domains [4,7–12,44–48]. To what extent the present model of NCLX_Mj is applicable to the native NCLX remains to be discovered.

4.7. Li^+-therapy and structure-dynamic determinants of ion selectivity in NCXL_Mj

The structure-dynamic determinants controlling the selectivity for Na^+ over Li^+ in Na^+-binding/transporting proteins remain unresolved [13,15,51–53]. Since the mitochondria are directly involved in the molecular mechanisms related with Li^+ therapy for bipolar disorders [54,55], resolution of the structure-dynamic relationships and functional properties of NCLX is of general interest. This has a practical significance since Li^+ therapy remains an effective treatment for decreasing the intracellular Na^+ and Ca^{2+} overloads in patients with bipolar disorders [54,55]. The present model of NCLX_Mj could be instrumental for elucidating the underlying mechanisms of Ca^{2+}, Na^+ and Li^+ discrimination at distinct sites. For example, the HDX-MS (Fig. 4) and mutational (Fig. 6) analyses revealed that the S_{Ca} site of NCLX_Mj can bind the Ca^{2+}, Na^+ or Li^+ ions, whereas the S_{Ca} site of NCX_Mj can bind either Ca^{2+} or Na^+ [21–25,31]. Interestingly enough, in NCX_Mj, four residues (T50, E54, T209 and E213) coordinating the Ca^{2+} ion at S_{Ca} are completely different from four residues (N50, D54, N209 and D213) located at the S_{Ca} site of NCLX_Mj (Fig. 1). The rearrangement of ion-coordinating residues at S_{Ca} of NCLX_Mj is very peculiar due to the replacement of two negatively charged residues (E) with shorter side-chain residues (D), whereas two carbonyl coordinating residues (T) are replaced by residues with more bulky (N) side-chains (Fig. 1B). Strikingly enough, this structural rearrangement at the S_{Ca} site has a relatively small effect on the K_m of Ca^{2+}, while aborting the ability of the S_{Ca} site to discriminate between the Na^+ and

Li^+ ions. The present model of NCLX_Mj in conjunction with cutting-edge experimental and computational approaches may lead to important conclusions regarding the fundamental issues dealing with the underlying mechanisms of monovalent/divalent ions segregation at "competing" and "noncompeting" sites [15,51–53].

Abbreviations

NCX	sodium-calcium exchanger
NCLX	mitochondrial NCX capable of Li^+ transport
CBD1 and CBD2	Ca^{2+} binding regulatory domains of eukaryotic NCXs
NCX_Mj	NCX from *Methanococcus jannaschii*
NCLX_Mj	the NCX_Mj-derived mutant protein capable of Li^+ transport
HDX-MS	Hydrogen-deuterium exchange mass spectrometry
TMRM	tetramethylrhodamine-5-maleimide
DMSO	Dimethyl sulfoxide
EGTA	Ethylene-bis(oxyethylenenitrilo)tetraacetic acid
MOPS	3-(*N*-morpholino) propanesulfonic acid
HEPES	4-(2-hydroxyethyl)-1-piperazineethanesulfonic acid
Bis-Tris propane	1,3-bis [tris-(hydroxymethyl)-methylamino]-propane
IPTG	Isopropyl β-D-1-thiogalactopyranoside
PMSF	phenylmethane sulfonyl fluoride
DTT	1,4-dithiothreitol
DDM	*n*-dodecyl-D-maltoside
DMPC	1,2-dimyristoyl-*sn*-glycero-3-phosphocholine
CHAPSO	3-([3-Cholamidopropyl] dimethylammonio)-2-hydroxy-1-propanesulfonate
POPG	1-palmitoyl-2-oleoyl-*sn*-glycero-3-phospho-(1′-rac-glycerol)
POPE	1-palmitoyl-2-oleoyl-sn-glycero-3-phosphoethanolamine.

Transparency document

The Transparency document associated with this article can be found, in online version.

CRediT authorship contribution statement

Moshe Giladi: Conceptualization, Data curation, Formal analysis, Writing - original draft. **Su Youn Lee:** Data curation, Formal analysis. **Bosmat Refaeli:** Data curation, Formal analysis. **Reuben Hiller:** Data curation, Formal analysis. **Ka Young Chung:** Conceptualization, Data curation, Funding acquisition, Supervision, Writing - original draft. **Daniel Khananshvili:** Conceptualization, Data curation, Supervision, Funding acquisition, Writing - original draft.

Acknowledgements

This work was partially supported by the Israel Science Foundation Grants #825/14 and #1351/18 to DK and by the National Research Foundation of Korea (NRF-2018R1A2B6001554 and NRF-2012R1A5A2A28671860) to KYC. The financial support of the Fields Estate Foundation to DK is highly appreciated. The Shmuel Shalit award to DK is gratefully aknnowledged.

Appendix A. Supplementary data

Supplementary data to this article can be found online at https://doi.org/10.1016/j.bbabio.2018.11.015.

References

[1] E. Carafoli, J. Krebs, Why calcium? How calcium became the best communicator, J. Biol. Chem. 291 (2016) 20849–20857.
[2] R. Filadi, E. Basso, K. Lefkimmiatis, T. Pozzan, Beyond intracellular signaling: the ins and outs of second messengers microdomains, Adv. Exp. Med. Biol. 981 (2017) 279–322.
[3] D. Khananshvili, The SLC8 gene family of sodium-calcium exchangers (NCX): structure, function, and regulation in health and disease, Mol. Asp. Med. 34 (2013) 220–235.
[4] R. Palty, I. Sekler, The mitochondrial Na^+/Ca^{2+} exchanger, Cell Calcium 52 (2012) 9–15.
[5] P.P. Schntkamp, A.H. Jalloul, G. Liu, R.T. Szerencsei, The SLC24 family of K^+-dependent Na^+-Ca^{2+} exchangers: structure-function relationships, Curr. Top. Membr. 73 (2014) 263–287.
[6] H.R. Zhekova, C. Zhao, P.P. Schnetkamp, S.Y. Noskov, Characterization of the cation binding sites in the NCKX2 Na^+/Ca^{2+}-K^+ exchanger, Biochemistry 55 (2016) 6445–6455.
[7] M. Giladi, I. Tal, D. Khananshvili, Structural features of ion transport and allosteric regulation in sodium-calcium exchanger (NCX) proteins, Front. Physiol. 7 (2016) 30, , https://doi.org/10.3389/fphys.2016.00030.
[8] M. Giladi, R. Shor, M. Lisnyansky, D. Khananshvili, Structure-functional basis of ion transport in sodium-calcium exchanger (NCX) proteins, Int. J. Mol. Sci. 17 (11) (2016) E1949, https://doi.org/10.3390/ijms17111949 pii.
[9] D. Khananshvili, Sodium-calcium exchangers (NCX): molecular hallmarks underlying the tissue-specific and systemic functions, Plügers Arch. 466 (2014) 43–60.
[10] K.D. Philipson, D.A. Nicoll, Sodium-calcium exchange: a molecular perspective, Annu. Rev. Physiol. 62 (2000) 111–133.
[11] M. Hilge, J. Aelen, G.W. Vuister, Ca^{2+} regulation in the Na^+/Ca^{2+} exchanger involves two markedly different Ca^{2+} sensors, Mol. Cell 22 (2006) 15–25.
[12] K. Bode, D.M. O'Halloran, NCX-DB: a unified resource for integrative analysis of the sodium-calcium exchanger super-family, BMC Neurosci. 19 (1) (2018) 1–10.
[13] I. Bahar, T.R. Lezon, L.W. Yang, E. Eyal, Global dynamics of proteins: bridging between structure and function, Annu. Rev. Biophys. 39 (2010) 23–42.
[14] E. Zomot, M. Gur, I. Bahar, Microseconds simulations reveal a new sodium-binding site and the mechanism of sodium-coupled substrate uptake by LeuT, J. Biol. Chem. 290 (2015) 544–555.
[15] B. Roux, S. Bernèche, B. Egwolf, B. Lev, S.Y. Noskov, C.N. Rowley, Y. Haibo, Ion selectivity in channels and transporters, J. Gen. Physiol. 137 (2011) 415–426, https://doi.org/10.1085/jgp.201010577.
[16] R. Palty, W.F. Silverman, M. Hershfinkel, T. Caporale, S.L. Sensi, J. Parnis, C. Nolte, D. Fishman, V. Shoshan-Barmatz, S. Herrmann, D. Khananshvili, I. Sekler, NCLX is an essential component of mitochondrial Na^+/Ca^{2+} exchange, Proc. Natl. Acad. Sci. U. S. A. 107 (2010) 436–441, https://doi.org/10.1073/pnas.0908099107.
[17] J.P. Reeves, C.C. Hale, The stoichiometry of the cardiac sodium-calcium exchange system, J. Biol. Chem. 259 (1984) 7733–7739.
[18] D.M. Bers, K.S. Ginsburg, Na:Ca stoichiometry and cytosolic Ca-dependent activation of NCX in intact cardiomyocytes, Ann. N. Y. Acad. Sci. 1099 (2007) 326–338.
[19] I. Shlosman, F. Marinelli, J.D. Faraldo-Gómez, J.A. Mindell, The prokaryotic Na^+/Ca^{2+} exchanger NCX_Mj transports Na^+ and Ca^{2+} in a 3:1 stoichiometry, J. Gen. Physiol. 150 (2018) 51–65.
[20] D. Khananshvili, Distinction between the two basic mechanisms of cation transport in the cardiac Na^+-Ca^{2+} exchange system, Biochemistry 29 (1990) 2437–2442.
[21] J. Liao, et al., Structural insight into the ion-exchange mechanism of the sodium/calcium exchanger, Science 335 (2012) 686–690.
[22] L. Almagor, et al., Functional asymmetry of bidirectional Ca^{2+}-movements in an archaeal sodium-calcium exchanger (NCX_Mj), Cell Calcium 56 (2014) 276–284.
[23] M. Giladi, L. Almagor, L. van Dijk, R. Hiller, P. Man, E. Forest, D. Khananshvili, Asymmetric preorganization of inverted pair residues in the sodium-calcium exchanger, Sci. Rep. 6 (2016) 20753, , https://doi.org/10.1038/srep20753.
[24] M. Giladi, L. van Dijk, B. Refaeli, L. Almagor, R. Hiller, P. Man, E. Forest, D. Khananshvili, Dynamic distinctions in the Na^+/Ca^{2+} exchanger adopting the inward- and outward-facing conformational states, J. Biol. Chem. 292 (2017) 12311–12323, https://doi.org/10.1074/jbc.M117.787168.
[25] F. Marinelli, L. Almagor, R. Hiller, M. Giladi, D. Khananshvili, J.D. Faraldo-Gómez, Sodium recognition by the Na^+/Ca^{2+} exchanger in the outward-facing conformation, Proc. Natl. Acad. Sci. U. S. A. 111 (2014) E5354–E5362.
[26] J. Liao, F. Marinelli, C. Lee, Y. Huang, J.D. Faraldo-Gómez, Y. Jiang, Mechanism of extracellular ion exchange and binding-site occlusion in a sodium/calcium exchanger, Nat. Struct. Mol. Biol. 23 (2016) 590–599.
[27] T. Nishizawa, S. Kita, A.D. Maturana, N. Furuya, K. Hirata, G. Kasuya, S. Ogasawara, N. Dohmae, T. Iwamoto, R. Ishitani, O. Nureki, Structural basis for the counter-transport mechanism of a H^+/Ca^{2+} exchanger, Science 341 (2013) 168–172.
[28] A.B. Waight, B.P. Pedersen, A. Schlessinger, M. Bonomi, B.H. Chau, Z. Roe-Zurz, A.J. Risenmay, A. Sali, R.M. Stroud, Structural basis for alternating access of a eukaryotic calcium/proton exchanger, Nature 499 (2013) 107–110.
[29] M. Wu, S. Tonga, S. Walterspergerb, K. Diederichsc, M. Wang, L. Zheng, Crystal structure of Ca^{2+}/H^+ antiporter protein YfkE reveals the mechanisms of Ca^{2+} efflux and its pH regulation, Proc. Natl. Acad. Sci. U. S. A. 110 (2013) 11367–11372.
[30] E. Carafoli, R. Tiozzo, G. Lugli, F. Crovetti, C. Kratzing, The release of calcium from heart mitochondria by sodium, J. Mol. Cell. Cardiol. 6 (1974) 361–371.
[31] B. Refaeli, M. Giladi, R. Hiller, D. Khananshvili, Structure-based engineering of Lithium-transport capacity in an archaeal sodium-calcium exchanger, Biochemistry 55 (2016) 1673–1676, https://doi.org/10.1021/acs.biochem.6b00119.
[32] Y. Nie, N. Ermolova, H.R. Kaback, Site-directed alkylation of LacY: effect of the proton electrochemical gradient, J. Mol. Biol. 374 (2007) 356–364, https://doi.org/10.1016/j.jmb.2007.09.006.
[33] X. Jiang, Y. Nie, H.R. Kaback, Site-directed alkylation studies with LacY provide evidence for the alternating access model of transport, Biochemistry 50 (2011) 1634–1640, https://doi.org/10.1021/bi101988s.
[34] M. Giladi, S.Y. Lee, Y. Ariely, Y. Teldan, R. Granit, R. Strulovich, Y. Haitin, K.Y. Chung, D. Khananshvili, Structure-based dynamic arrays in regulatory domains of sodium-calcium exchanger (NCX) isoforms, Sci. Rep. 7 (1) (2017) 993, https://

doi.org/10.1038/s41598-017-01102.
[35] M. Giladi, S.Y. Lee, R. Hiller, K.Y. Chung, D. Khananshvili, Structure-dynamic determinants governing a mode of regulatory response and propagation of allosteric signal in splice variants of Na^+/Ca^{2+} exchange (NCX) proteins, Biochem. J. 465 (2015) 489–501.
[36] S.Y. Lee, M. Giladi, H. Bohbot, R. Hiller, K.Y. Chung, D. Khananshvili, Structure-dynamic basis of splicing dependent regulation in tissue-specific variants of the sodium-calcium exchanger (NCX1), FASEB J. 30 (2016) 1356–1366.
[37] D. Khananshvili, E. Weil-Maslansky, D. Baazov, Kinetics and mechanism: modulation of ion transport in the cardiac sarcolemma sodium-calcium exchanger by protons, monovalent ions and temperature, Ann. N. Y. Acad. Sci. 779 (1996) 217–235.
[38] D. Khananshvili, Voltage-dependent modulation of ion-binding and translocation in the cardiac Na^+-Ca^{2+} exchanger, J. Biol. Chem. 266 (1991) 13764–13769.
[39] D. Khananshvili, E. Weil-Maslansky, The cardiac Na^+-Ca^{2+} exchanger: relative rates of calcium and sodium movements and their modulation by protonation-deprotonation of the carrier, Biochemistry 33 (1994) 312–319.
[40] D. Khananshvili, G. Shaulov, E. Weil-Maslansky, Rate-limiting mechanisms of exchange reactions in the cardiac sarcolemma Na^+-Ca^{2+} exchanger, Biochemistry 33 (1995) 10290–10297.
[41] D.W. Hilgemann, D.A. Nicoll, K.D. Philipson, Charge movement during Na^+-translocation by native and cloned Na^+/Ca^{2+} exchanger, Nature 352 (1991) 715–718.
[42] S. Matsuoka, D.W. Hilgemann, Steady-state and dynamic properties of cardiac sodium-calcium exchange. Ion and voltage dependencies of the transport cycle, J. Gen. Physiol. 100 (1992) 963–1001.
[43] A.H. Jalloul, S. Cai, R.T. Szerencsei, P.P.M. Schnetkamp, Residues important for K^+ ion transport in the K^+-dependent Na^+-Ca^{2+} exchanger (NCKX2), Cell Calcium 74 (2018) 61–72.
[44] D. Khananshvili, Long-range allosteric regulation of pumps and transporters: what can we learn from mammalian NCX antiporters, Adv. Biochem. Health Disease 14 (2016) 93–115.
[45] D. Khananshvili, Structure-dynamic coupling through Ca^{2+}-binding regulatory domains of mammalian NCX isoform/splice variants, Adv. Exp. Med. Biol. 981 (2018) 41–58.
[46] A. Verkhratsky, M. Trebak, F. Perocchi, D. Khananshvili, I. Sekler, Crosslink between calcium and sodium signalling, Exp. Physiol. 103 (2018) 157–169.
[47] J. Lytton, Na^+/Ca^{2+} exchangers: three mammalian gene families control Ca^{2+} transport, Biochem. J. 406 (2007) 365–368.
[48] T.S. Luongo, et al., The mitochondrial Na^+/Ca^{2+} exchanger is essential for Ca^{2+} homeostasis and viability, Nature 545 (2017) 93–97.
[49] Carafoli, The fateful encounter of mitochondria with calcium: how did it happen? Biochim. Biophys. Acta 1797 (2010) 595–606.
[50] L. Boyman, G.S.B. Williams, D. Khananshvili, I. Sekler, W.J. Lederer, NCLX: the mitochondrial sodium calcium exchanger, J. Mol. Cell. Cardiol. 59 (2013) 205–213.
[51] H.R. Zhekova, V. Ngo, M.C. Da Silva, D.R. Salahub, S.Y. Noskov, Selective ion binding and transport by membrane proteins – a computational perspective, Coord. Chem. Rev. 345 (2017) 108–136.
[52] N. Manin, M.C. da Silva, I. Zdravkovic, O. Eliseeva, A. Dyshin, O. Yaşar, D.R. Salahub, A.M. Kolker, M.G. Kiselev, S.Y. Noskov, LiCl solvation in *N*-methyl-acetamide (NMA) as a model for understanding Li^+ binding to an amide plane, Phys. Chem. Chem. Phys. 18 (2016) 4191–4200.
[53] T. Dudev, K. Mazmanian, C. Lim, Competition between Li^+ and Na^+ in sodium transporters and receptors: which Na^+-binding sites are “therapeutic” Li^+ targets? Chem. Sci. 9 (17) (2018) 4093–4103.
[54] E. Jakobsson, O. Argüello-Miranda, S.W. Chiu, Z. Fazal, J. Kruczek, S. Nunez-Corrales, S. Pandit, L. Pritchet, Towards a unified understanding of lithium action in basic biology and its significance for applied biology, J. Membr. Biol. 250 (2017) 587–604.
[55] T. Kato, Neurobiological basis of bipolar disorder: Mitochondrial dysfunction hypothesis and beyond, Schizophr. Res. 187 (2017) 62–66.
[56] L. van Dijk, M. Giladi, B. Refaeli, R. Hiller, M.H. Cheng, I. Bahar, D. Khananshvili, Key residues controlling bidirectional ion movements in Na^+/Ca^{2+} exchanger, Cell Calcium 76 (2018) 10–22.